Defining Metabolic Zonation as a Determinant of Hepatocyte Plasticity

Caitlin McCaffrey, Kyle Davies, Luke Boulter, Rachel Guest

University of Edinburgh, Institute of Genetics and Cancer

cmccaff3@ed.ac.uk

Introduction

The mechanisms underlying biliary epithelial cell (BEC) repopulation and repair following hepatic injury are crucial for understanding both liver regeneration and the origins of diseases such as cholangiocarcinoma (CCA). Experimental data has shown that under certain circumstances, specifically following up-regulation of the Notch signalling pathway, hepatocytes can transdifferentiate into BECs[1]. The underlying mechanisms driving this cell fate transition are poorly understood. In particular, it is unknown whether all hepatocytes across the liver lobule have inherent capacity for this plasticity or whether liver zonation plays a role in determining such changes in cell identity.

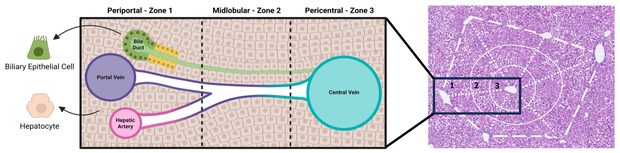

Figure 1: Micro-architecture of the Liver. *Representative H&E-stained liver demonstrating the microscopic structure of the hepatic lobules which are composed of several portal triads comprising bundles of bile ductules and branches of the hepatic artery and portal vein radiate out from a central vein. The lobule is subdivided into 3 zones, the periportal zone 1, midlobular zone 2, and pericentral zone 3. The functional characteristics of hepatocytes are defined by their zonal origin (Schematic created with BioRender.com).*

Hypothesis:
Metabolic zonation is a key determinant of hepatocyte plasticity

Aims:

- Determine whether hepatocyte reprogramming is zone-dependent by comparing periportal ($Gls2^+$) and pericentral (GS^+) hepatocyte responses to NICD1/Akt in vivo.
- Determine if hepatocyte zonation is maintained in culture and whether liver cell reprogramming can be modelled *ex vivo*.

NICD1/AKT Upregulation Induces Hepatocyte-Derived Biliary Neoplasm Formation

This study used hydrodynamic tail vein injection (HTVI, *Figure 2a*)[2] to deliver NICD1 and AKT to hepatocytes via the Sleeping Beauty transposon system. Four weeks later, transduced hepatocytes showed striking plasticity, converting from large multinucleate polygonal cells into condensed columnar mononuclear cells that formed lumen-like bile ductule structures (*Figure 2b-f*) and expressed biliary markers such as cytokeratin 19 (K19).

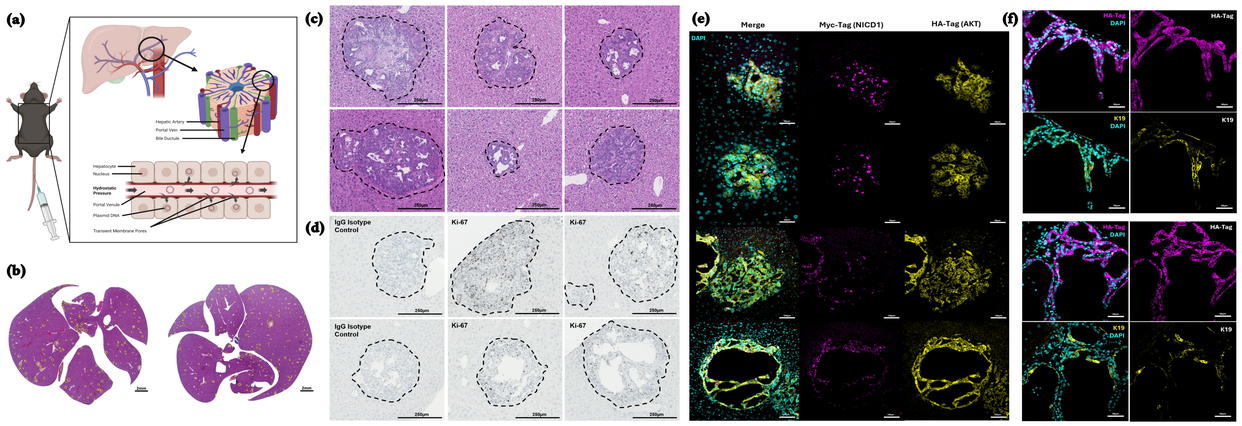

Figure 2: Hepatocytes Form Biliary Neoplasms Following The Upregulation of NICD1/AKT Signalling Via HTVI. ***(a)*** *Schematic of hydrodynamic tail vein injection, in which a rapid bolus of plasmid solution transiently increases venous and sinusoidal pressure, enabling plasmid uptake by hepatocytes (Schematic created with BioRender.com).* ***(b)*** *Representative H&E-stained whole-liver sections from C57Bl6/J wild-type mice 4 weeks after NICD1/Akt HTVI, showing multiple hepatocyte-derived biliary neoplasms (yellow outlines).* ***(c)*** *High-magnification H&E-stained images of individual neoplastic lesions (dashed outlines).* ***(d)*** *DAB-stained sections demonstrating increased nuclear Ki-67 immunoreactivity in biliary neoplasms compared with IgG isotype controls (dashed outlines).* ***(e)*** *Immunofluorescent staining confirming dual expression of Myc-tagged NICD1 and HA-tagged Akt within HTVI-induced biliary neoplasms.* ***(f)*** *Immunofluorescent staining showing co-localization of HA-tagged Akt with the mature biliary epithelial cell marker cytokeratin 19 (K19) in biliary neoplasms.*

NICD1/AKT-Induced Biliary Neoplasms Originate from Gls2-Expressing Hepatocytes

It was evident that the overexpression of NICD1/AKT induced phenotypic remodelling in the mGFP-marked **Gls2-expressing periportal hepatocytes**, whilst inducing the expression of Sox9, an early transcriptional regulator of BEC lineage commitment (*Figure 4a-b*).

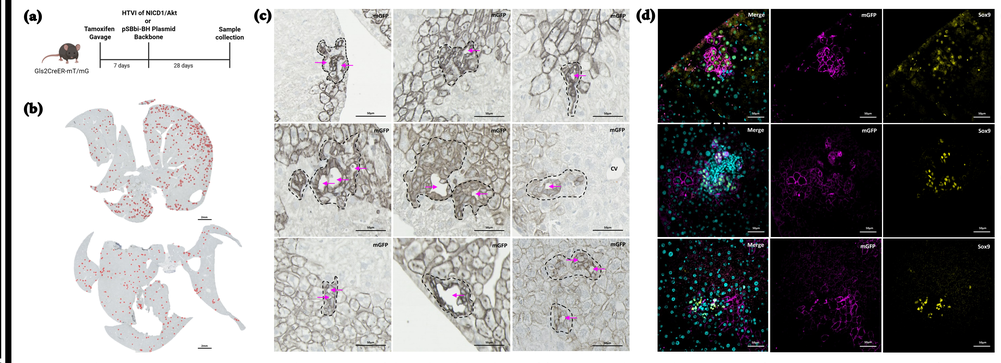

Figure 4: Gls2-expressing Hepatocytes Contribute to NICD1/Akt-Induced Neoplasms. ***(a)*** *Timeline of tamoxifen and NICD1/Akt HTVI in Gls2CreER-mT/mG mice (n=4) (Schematic created with BioRender.com).* ***(b)*** *DAB-stained livers 7 days post-HTVI showing biliary neoplasm number and distribution (red highlights).* ***(c)*** *mGFP DAB 4 weeks post-HTVI showing altered morphology and lumen formation in recombined hepatocytes.* ***(d)*** *mGFP and Sox9 immunofluorescence 4 weeks post-HTVI showing Gls2-lineage contribution to $Sox9^+$ biliary-like structures.* ***(e)*** *Volcano plot of differentially expressed genes in $mGFP^+$ hepatocytes from plasmid backbone- versus NICD1/Akt-treated mice (DESeq2; adjusted $p < 0.05$; $|log_2FC| > 1$).* ***(f)*** *Gene Ontology (GO) enrichment of differentially expressed genes (adjusted $p < 0.05$), filtered to GO terms occurring in >5% of genes. Bubble size reflects the number of genes per term; colour (cyan–magenta) reflects q-value. BP = Biological Processes; MF = Molecular Functions.*

Conversely, **GS-expressing pericentral hepatocytes** exhibited no detectable participation in biliary neoplasm formation despite confirmed plasmid uptake (*Figure 5b*). Interestingly, GS+ hepatocytes were observed to be in direct contact with NICD1/AKT-driven neoplasms, yet lineage-traced recombined cells remained absent from these lesions, suggesting strict lineage restriction despite microenvironmental proximity (*Figure 5c-d*).

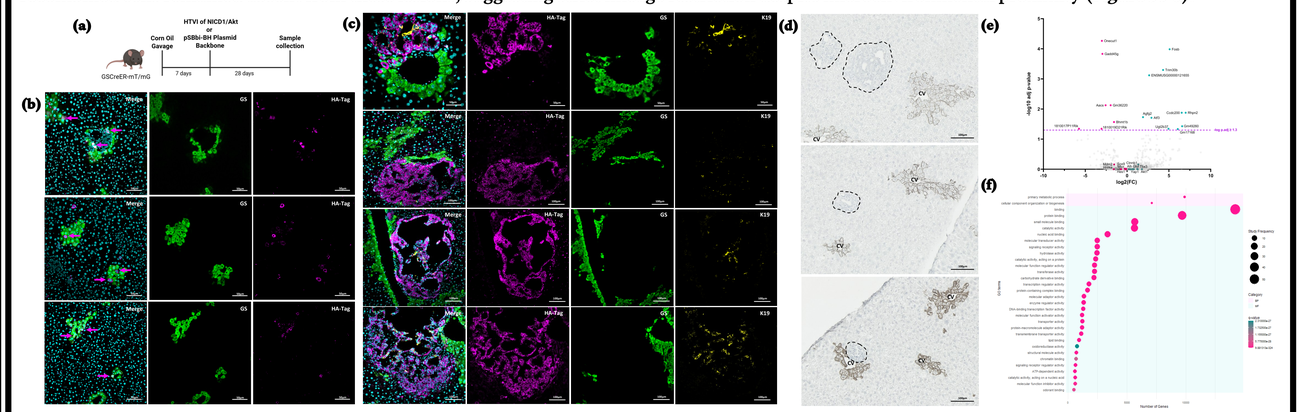

Figure 5: GS-expressing Hepatocytes Resist NICD1/Akt-driven Phenotypic Changes. ***(a)*** *Timeline of corn oil and NICD1/Akt HTVI in GSCreER-mT/mG mice (n=4) (Schematic created with BioRender.com).* ***(b)*** *Immunofluorescence confirming plasmid uptake (HA, magenta) in GS^+ cells (green)* ***(c)*** *GS^+ cells near HA^+ neoplastic lesions with $K19^+$ biliary regions (yellow).* ***(d)*** *mGFP DAB in NICD1/Akt-treated GSCreER-mT/mG mice (n=5) showing unchanged morphology of recombined hepatocytes (biliary neoplasms in black).* ***(e)*** *Volcano plot of differentially expressed genes in $mGFP^+$ hepatocytes from backbone- versus NICD1/Akt-treated mice (DESeq2; adjusted $p < 0.05$; $|log_2FC| > 1$).* ***(f)*** *GO enrichment of differentially expressed genes (adjusted $p < 0.05$), filtered for GO terms occurring in >5% of genes. Bubble size reflects the number of genes per term; colour (cyan–magenta) reflects q-value. BP = Biological Processes; MF = Molecular Functions.*

Zonated Lineage-Tracing Gls2CreER-mT/mG and GSCreER-mT/mG Mouse Models

Two tamoxifen-inducible, zone-specific lineage-tracing models were generated by crossing Gls2CreER or GSCreER mice with the mT/mG reporter. Cre activation switches membrane fluorescence from Tomato (red) to GFP (green) in Gls2+ periportal or GS+ pericentral hepatocytes, enabling permanent labelling of zone 1 and zone 3 cells.

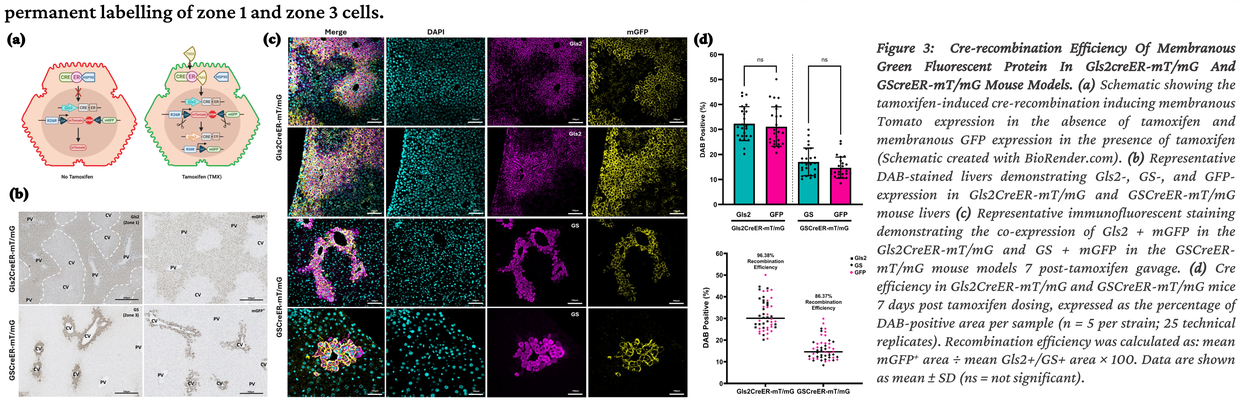

Figure 3: Cre-recombination Efficiency Of Membranous Green Fluorescent Protein In Gls2creER-mT/mG And GScreER-mT/mG Mouse Models. ***(a)*** *Schematic showing the tamoxifen-induced cre-recombination inducing membranous Tomato expression in the absence of tamoxifen and membranous GFP expression in the presence of tamoxifen (Schematic created with BioRender.com).* ***(b)*** *Representative DAB-stained livers demonstrating Gls2-, GS-, and GFP-expression in Gls2CreER-mT/mG and GScreER-mT/mG mouse livers* ***(c)*** *Representative immunofluorescent staining demonstrating the co-expression of Gls2 + mGFP in the Gls2CreER-mT/mG and GS + mGFP in the GScreER-mT/mG mouse models 7 post-tamoxifen gavage.* ***(d)*** *Cre efficiency in Gls2CreER-mT/mG and GScreER-mT/mG mice 7 days post tamoxifen dosing, expressed as the percentage of DAB-positive area per sample (n = 5 per strain; 25 technical replicates). Recombination efficiency was calculated as: mean $mGFP^+$ area ÷ mean Gls2+/GS+ area × 100. Data are shown as mean ± SD (ns = not significant).*

3D-Cultured Hepatocytes Maintain Functionality and Zonation

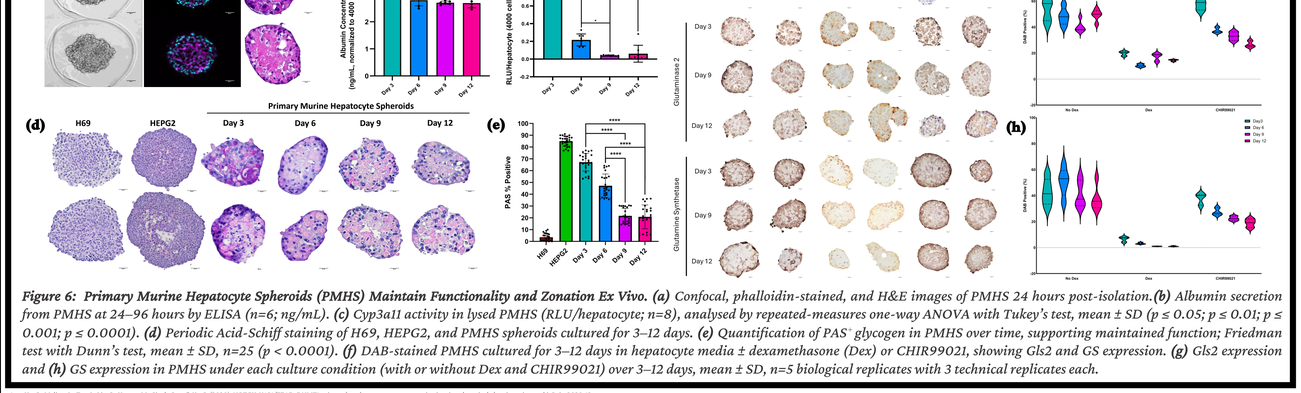

Figure 6: Primary Murine Hepatocyte Spheroids (PMHS) Maintain Functionality and Zonation Ex Vivo. ***(a)*** *Confocal, phalloidin-stained, and H&E images of PMHS 24 hours post-isolation.* ***(b)*** *Albumin secretion from PMHS at 24–96 hours by ELISA (n=6; ng/mL).* ***(c)*** *Cyp3a11 activity in lysed PMHS (RLU/hepatocyte; n=8), analysed by repeated-measures one-way ANOVA with Tukey's test, mean ± SD ($p \leq 0.05$; $p \leq 0.01$; $p \leq 0.001$; $p \leq 0.0001$).* ***(d)*** *Periodic Acid-Schiff staining of H69, HEPG2, and PMHS spheroids cultured for 3–12 days.* ***(e)*** *Quantification of PAS^+ glycogen in PMHS over time, supporting maintained function; Friedman test with Dunn's test, mean ± SD, n=25 ($p < 0.0001$).* ***(f)*** *DAB-stained PMHS cultured for 3–12 days in hepatocyte media ± dexamethasone (Dex) or CHIR99021, showing Gls2 and GS expression.* ***(g)*** *Gls2 expression and* ***(h)*** *GS expression in PMHS under each culture condition (with or without Dex and CHIR99021) over 3–12 days, mean ± SD, n=5 biological replicates with 3 technical replicates each.*

1. Hu, S., Molina, L., Tao, J., Liu, S., Hassan, M., Singh, S., ... & Ko, S. (2020). NOTCH-YAP1/TEAD-DNMT1 axis regulates hepatocyte reprogramming into intrahepatic cholangiocarcinoma. bioRxiv, 2020-12.
2. Bualbet, V., Zhang, G., Danko, I., Williams, P., & Wolff, J. (1998). The efficient expression of intravascularly delivered DNA in rat muscle. Gene therapy, 5(2), 272-276.